Analysis of the Seasonal Variation in Atmospheric NH_3 over East Asia

Wang, Zhe
Research Institute for Applied Mechanics, Kyushu University | Institute of Atmospheric Physics, Chinese Academy of Sciences, Beijing

Uno, Itsushi
Research Institute for Applied Mechanics, Kyushu University : Professor

Osada, Kazuo
Graduate School of Environmental Studies, Nagoya University

Itahashi, Syuichi
Central Research Institute of Electric Power Industry

他

Analysis of the Seasonal Variation in Atmospheric NH₃ over East Asia

Zhe WANG[*1, 2], Itsushi UNO[*1], Kazuo OSADA[*3], Syuichi ITAHASHI[*4],

Keiya YUMIMOTO[*1] and Shigekazu YAMAMOTO[*5]

E-mail of corresponding author: *uno@riam.kyushu-u.ac.jp*

Abstract

Atmospheric ammonia (NH₃) plays an important role in the formation and understanding of secondary inorganic aerosols, but has not been examined using chemical transport models (CTMs) and atmospheric levels have not been compared with satellite observations. Here, we analyzed the seasonal variation in atmospheric NH₃ using long-term hourly NH_3/NH_4^+ measurements made at the Chikushi Campus of Kyushu University in Fukuoka, nationwide filter pack (FP) network observations over Japan, GEOS-Chem CTM results, and Infrared Atmospheric Sounding Interferometer (IASI) satellite retrievals over East Asia. We found that the IASI NH₃ retrieval over central and north China had a strong correlation with the CTM results (R = 0.74). There was a similar correlation over south China, but the IASI NH₃ retrieval was only 48% of the CTM value. CTM results over Japan reproduced the major seasonal variations compared with surface observations, but IASI observations over Japan were below or near the detection limit and it was difficult to obtain a reasonable correlation with measurements.

1. Introduction

Due to its significant impact on human health and climate, atmospheric aerosol has become an important environmental issue at the global and regional scales, especially over East Asia. Atmospheric ammonia (NH₃) plays an important role in understanding the formation of secondary inorganic aerosols, which are important components of atmospheric aerosol. Ammonia is a highly reactive gas and can form secondary ammonium (NH_4^+), which is the most important cation, via reactions with acidic gases formed from nitrogen oxides (NO_x), sulfur dioxide (SO_2), and hydrochloric acid (HCl) [1].

Because it is a soluble alkaline gas and can react rapidly with acid gases, atmospheric NH₃ also has an important influence on the acidity of precipitation [2]. Through wet and dry deposition processes, NH₃ and its derivatives are deposited in ecosystems, increasing

eutrophication and reducing biodiversity [3]. In recent decades, NH₃ emissions have increased substantially due to intensive livestock production and the use of fertilizers.

Despite the importance of NH₃ in the environment, the atmospheric processes controlling NH₃ levels and its related budgets are still poorly understood [1]. This is because the measurement of NH₃ is challenging due to the following: (i) strong temporal and spatial variability of ambient levels, (ii) rapid conversion of NH₃ between phases (gas/particulate/liquid), and (iii) its tendency to adhere to the surfaces of measurement instruments [4]. There are currently very few monitoring stations that provide daily or hourly resolved NH₃ measurements, with most long-term monitoring of NH₃ conducted using a passive sampler or dedicated denuder at a time resolution of several weeks.

In addition to the direct measurement of NH₃, chemical transport models (CTMs) are useful tools for studying the sources and sinks of NH₃, and the processes controlling its levels in the atmosphere. However, model results may have a large bias due to uncertainties of emissions and atmospheric processes; therefore, they require careful evaluation. Over the last few years, satellite instruments capable of detecting NH₃ vertical

*1 Research Institute for Applied Mechanics, Kyushu Univ.

*2 Institute of Atmospheric Physics, Chinese Academy of Sciences, Beijing, China

*3 Graduate School of Environmental Studies, Nagoya Univ.

*4 Central Research Institute of Electric Power Industry

*5 Fukuoka Institute of Health and Environmental Sciences

column density (VCD) have been used to study the emission, distribution, and transport of NH_3 at global and regional scales [5, 6]. Satellite data also require careful evaluation due to the large relative errors, especially in areas with low VCD.

In this study, we analyzed the seasonal variation in atmospheric NH_3 using hourly NH_3/NH_4^+ measurements at Chikushi Campus of Kyushu University (CC-KU) in Fukuoka, nationwide filter pack (FP) network observations over Japan, GEOS-Chem CTM results, and satellite measurements over East Asia.

2.   Observations

2.1 Surface Measurement

Concentrations of gaseous NH_3 and aerosol NH_4^+ were measured using a semi-continuous microflow analytical system (MF-NH_3A; Kimoto Electric Co. Ltd., Osaka, Japan) located on the sixth floor of G building in the CC-KU (33.52°N, 130.47°E). Atmospheric NH_3 and NH_4^+ (Dp < 2.0 µm) were measured hourly between July 31, 2014 and October 19, 2015. The details of the observation system and basic data analysis have been reported previously [7-9].

2.2   Japan   Environmental   Laboratories Association (JELA) aerosol observation

We used the observation dataset (from 2010 to 2014) of the JELA, which was acquired at 33 sites in Japan [10]. The JELA dataset provides monthly averaged atmospheric aerosol and gas concentrations measured by the FP method. We used the NH_3 concentration for our analysis (hereafter denoted as FP data) and excluded sites where there was a strong local influence from agriculture and livestock farming. Figure 5 shows the observation sites used in this study and Table 1 shows the site used for a time series comparison (Figs. 6–8).

2.3 Satellite Retrieval

The improved Infrared Atmospheric Sounding Interferometer (IASI) NH_3 data set was used in this study. IASI is a passive remote-sensing instrument, operating in nadir mode that measures the infrared radiation emitted by the Earth's surface and atmosphere [9]. The algorithm used to retrieve NH_3 columns from the radiance spectra is described in detail and compared to previous algorithms in literature [11]. The NH_3 columns

Table 1 Japan Environmental Laboratories Association (JELA) filter pack (FP) NH_3 sites used for a time series comparison

Region	Site	No.	Lat.	Lon.
Hokkaido	Rishiri	S1	45.12°N	141.21°E
Hokkaido	Moshiri	S2	44.36	142.27
Kanto	Kazo	S8	36.09	139.56
Kanto	Ichikawa	S9	35.72	139.93
Kanto	Ichihara	S10	35.53	140.07
Kanto	Sakura	S13	35.73	140.21
Kyushu	Dazaifu (FIHES)	S26	33.51	130.50
Kyushu	Fukuoka	S27	33.50	130.31
Kyushu	Oita-Kuju	S28	33.04	131.25
Kyushu	Oita	S29	33.16	131.61
Kyushu	Miyazaki	S30	31.83	131.42
Kyushu	Kagoshima	S31	31.35	130.34

were retrieved based on the hyperspectral range index (HRI, a dimensionless spectral index from IASI Level 1C radiance), thermal contrast (TC, temperature difference between the earth's surface and the atmosphere at 1.5 km from the IASI Level 2 information), and look-up tables (LUTs, built from forward radiative transfer model simulations). The relative errors were estimated by considering the uncertainties of HRI and TC, with large errors related to low values of HRI (indicating low values of the NH_3 column) and/or TC.

The IASI instrument is on board the polar sun synchronous MetOp platform, which crosses the equator at a mean local solar time of 9.30 a.m and p.m. It therefore allows global retrievals of NH_3 twice a day. In this study, we only considered the measurements from the morning overpass because they are generally more sensitive to NH_3 and have smaller relative errors due to the higher TC at this time of day [11]. The availability of measurements was mainly controlled by the cloud cover, with only observations with cloud cover lower than 25% being processed. It has be showed that given the strong dependence on TC, the spring–summer months are better suited to accurately measure NH_3 from IASI (error below 50%) [12]. As an example of the detection limit (defined as 2σ on the HRI) for an individual observation, a NH_3-retrieved column was considered detectable when the column exceeded 9.68×10^{15} molecules cm^{-2} (surface concentration exceeded 1.74 µg m^{-3}) at a TC of 20 K, while the column should be larger than 1.69×10^{16} molecules cm^{-2} (3.05 µg m^{-3}) at 10 K [12].

In this study, the IASI-NH₃ observations were produced at the Université Libre de Bruxelles (ULB), and were taken from a dataset located at http://www.pole-ether.fr/etherTypo/index.php?id=1700 &L=1. The dataset includes: (1) the ammonia total column along the satellite swath path (data only for conditions with cloud cover < 25%), (2) error on the ammonia total column, (3) cloud cover on ground pixels, (4) vertical profile used in the retrieval procedure, and (5) viewing angle of the satellite. Ammonia total column data (i.e., VCD) were then re-gridded to the GEOS-Chem Asian grid system with $0.5° \times 0.667°$ resolution.

3. Numerical Model and Emission Inventory

We used the three-dimensional (3-D) Goddard Earth Observing System - Chemistry (GEOS-Chem) CTM (ver. 09-02) [13,14]. The model was run with the full GEOS-Chem NOx-Ox-VOC-HOx-CO chemistry option to simulate the formation of aerosols, including mineral dust, sea salt, and secondary inorganic aerosols. We also modeled the emission/transport of primary black carbon (BC) and organic carbon (OC). The model used the assimilated meteorological fields from the GEOS of the NASA Global Modeling and Assimilation Office (GMAO). The model has a horizontal resolution of $2° \times 2.5°$ for global runs, and $0.5° \times 0.667°$ for Asian one-way nesting runs (11°S−55°N, 70−150°E), with both having 47 vertical levels from the surface to 0.01 hPa. The lowest model layer thickness was approximately 130 m. We used anthropogenic emissions data from the Emission Database for Global Atmospheric Research (EDGAR) [15] for the global domain and the Regional Emission Inventory in Asia (REAS) (ver. 2.1) for the Asian domain [16]. REAS NH₃ emissions were modified to include seasonal variations in Asia based on the literature [17] and the changes in winter emissions recommended by the literature [18]. The model simulation covered the period from the beginning of December 2013 to October 2015. Other basic numerical settings were as reported previously [19, 20].
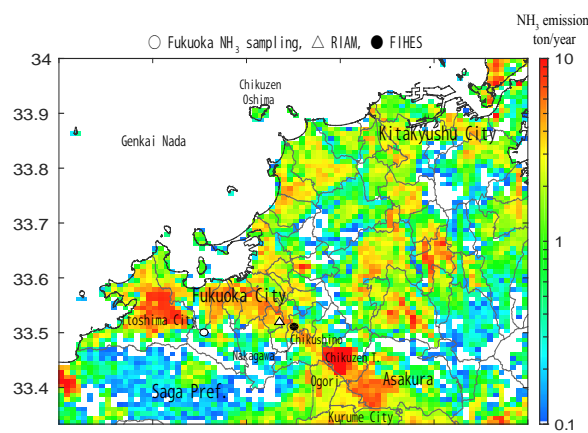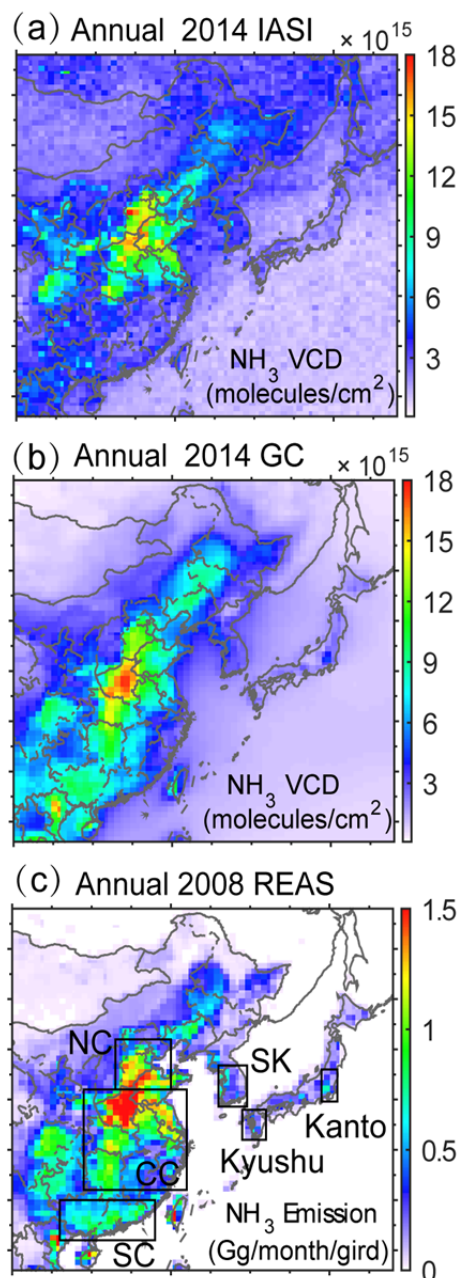

Fig. 2 Annual averaged distribution of (a) IASI NH₃ VCD, (b) GEOS-Chem simulated NH₃ VCD, (c) REAS NH₃ emission intensity. Grid = $0.5° \times 0.667°$.

Fig. 1 Observation sites (RIAM, Dazaifu-FIHES, and Fukuoka FP) and an NH₃ emission intensity map (1 × 1 km resolution).

4. Results and Discussion

Figure 1 shows the NH$_3$ emission map for Fukuoka Prefecture (1 × 1 km resolution) from the EAGrid data base [21] and observation sites. The open triangle shows our observation site (Chikushi). Open and closed circles (open circles = S27 are Fukuoka city group measurement sites, and closed circles = S26 are Dazaifu-FIHES group measurement sites) show the FP-NH$_3$ measurement sites used to compare observation and model results. The high NH$_3$ emission 5–10 km south of the observation sites (CC-KU and FIHES) may have influenced measurements, with NH$_3$ emission mainly originating from local agriculture and poultry farming (See Fig. 1 and Appendix A3).

4.1 Seasonal/Horizontal Distribution of NH$_3$ Column Density

Figure 2 shows a comparison of the annual average concentration from IASI and GEOS-Chem model results, and also shows the annual averaged NH$_3$ emission from the REAS inventory. Figure A1 shows the number of observation data points, averaged cloud cover, and relative error. Both IASI and GEOS-Chem data show a
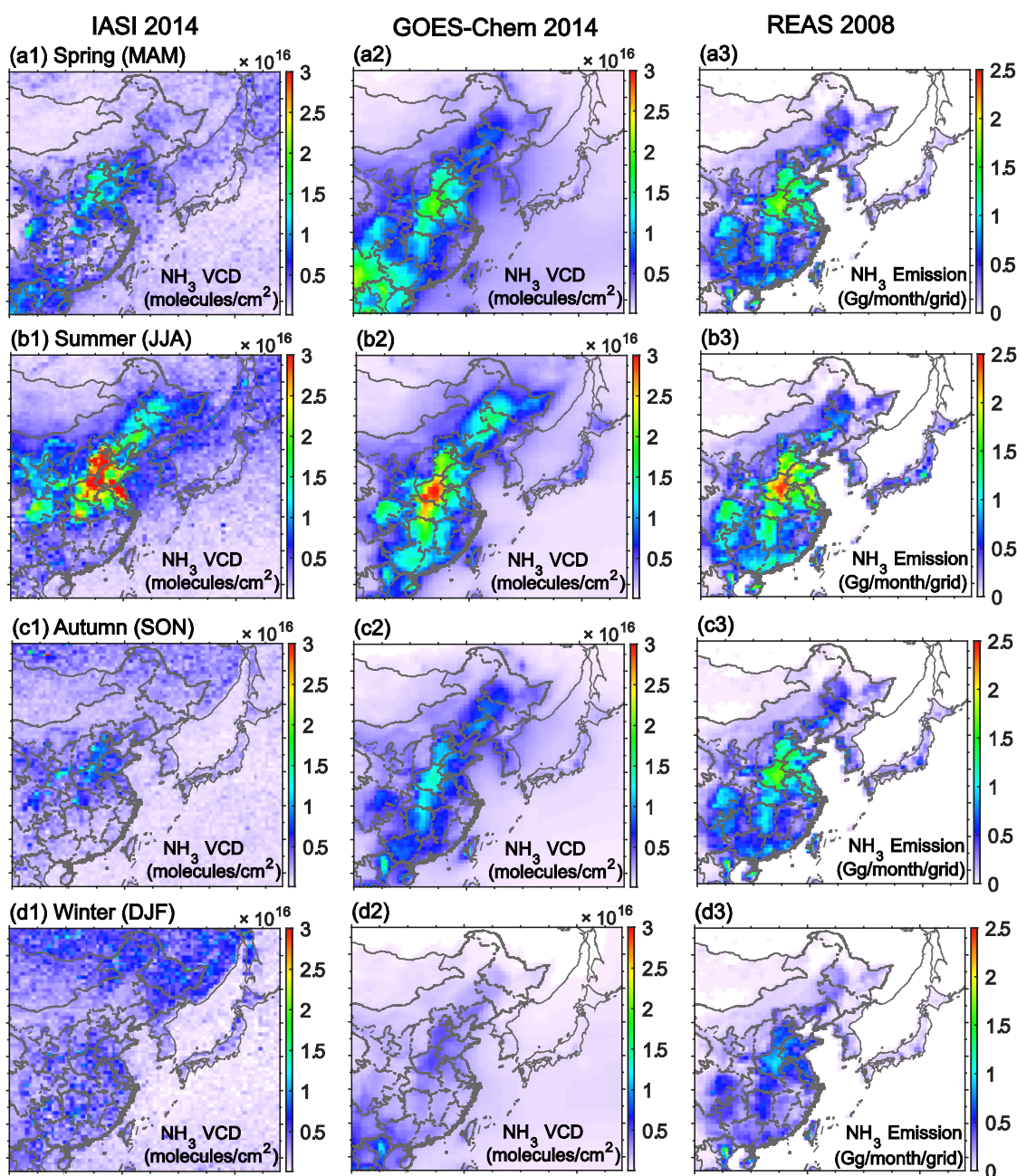

Fig. 3 Same as Figure 2, but for different seasons. Grid = 0.5° × 0.667°.

high NH$_3$ VCD over north (Beijing, Tianjin, and the south of Hebei province) and central (Henan and Hubei provinces) China, where the annual mean NH$_3$ VCD could reach 1.5×10^{16} molecules cm^{-2}. The relative errors over these regions were small (<150%) due to the high NH$_3$ value. Over south China, the IASI NH$_3$ VCD was significantly lower than the GEOS-Chem value due to the small number of measurements, high levels of cloud cover, and large relative errors. The NH$_3$ VCD

was less than 6×10^{15} molecules cm^{-2} over all of Japan. The relative error over Japan was higher than that over central China due to the lower NH$_3$ VCD. The IASI NH$_3$ VCD was below or near the detection limit (as discussed in Section 2.3), except over north and central China. The GEOS-Chem NH$_3$ was consistent with REAS NH$_3$ emissions, indicating the importance of local emissions on the NH$_3$ VCD at the annual scale.
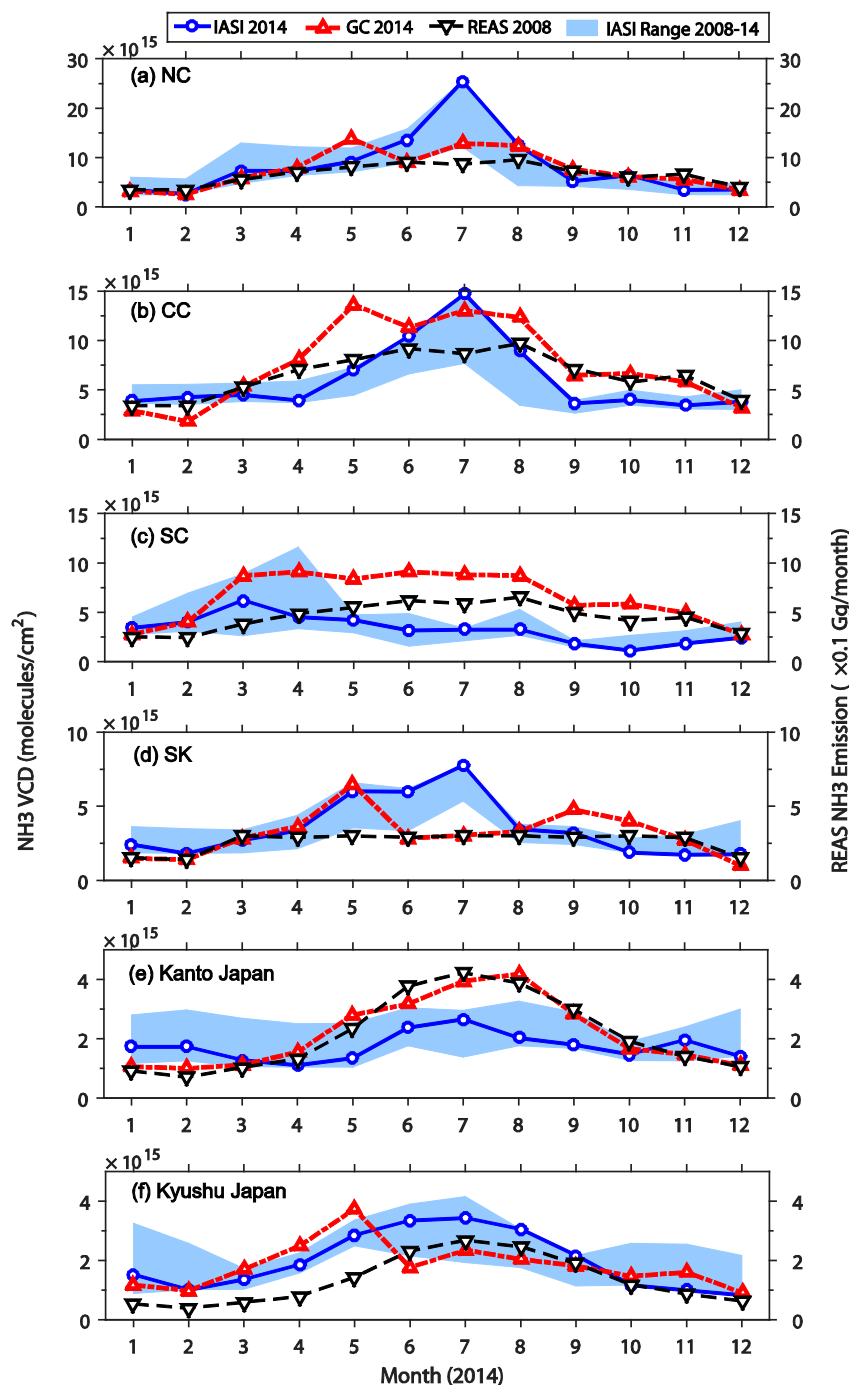
Figures 3 and A2 show the same elements as Figs. 2

Fig. 4 Region-averaged monthly time series of IASI NH$_3$ VCD (shade), GEOS-Chem NH$_3$ VCD (red dashed line), and REAS NH$_3$ emissions (black dashed line with open triangles).

and A1, respectively, but in each different season (SON, DJF, MAM, and JJA). The horizontal distributions of the IASI and GEOS-Chem NH$_3$ VCD were generally similar in the different seasons when expressed as an annual mean, with high values over north and central China. However, the GEOS-Chem results revealed that the areas downwind of China (e.g., the East China Sea and Japan sea areas) had a higher NH$_3$ VCD in spring than in summer, even though the NH$_3$ VCD over China was significantly higher in summer than in spring. This indicates the importance of long-range transport of NH$_3$ over East Asia in the cold season when northwest winds are dominant. The seasonal variations were significant and consistent in the IASI and GEOS-Chem results, with higher values of 3×10^{16} molecules cm^{-2} (central China) in summer and lower values of about 5×10^{15} molecules cm^{-2} in winter. Due to the low NH$_3$ VCD, IASI retrievals had larger relative errors (>150%) in winter over the East Asia area. Over Japan, IASI retrievals did not display seasonal variation due to the large relative errors, while GEOS-Chem produced a higher NH$_3$ VCD in summer than in winter.

Figure 4 shows the region-averaged monthly time series of ISAI NH$_3$ VCD, GEOS-Chem NH$_3$ VCD, and REAS NH$_3$ emissions for the six regions shown in Fig. 2. North China had a clear summer peak of NH$_3$ VCD in IASI retrievals and GEOS-Chem results, but the GEOS-Chem peak in July (1.2×10^{16} molecules cm^{-2}) was lower than the IASI peak (2.6×10^{16} molecules cm^{-2}), which may be due to the underestimation of NH$_3$ emissions. The pattern of IASI NH$_3$ seasonal variation over central China was similar to that over north China, and the GEOS-Chem results also indicated a similar seasonal variation. However, the IASI NH$_3$ level over north China (maximum: 2.6×10^{16} molecules cm^{-2}) was significantly higher than that over central China (maximum: 1.5×10^{16} molecules cm^{-2}), while the

GEOS-Chem results indicated a similar NH$_3$ level (maximum: 1.4×10^{16} molecules cm^{-2}). As a result, GEOS-Chem NH$_3$ levels in July were consistent with those of IASI retrievals, but were higher than IASI levels in May. GEOS-Chem NH$_3$ results over south China were higher than IASI retrievals in spring and summer; however, the IASI data did not reveal clear seasonal variation due to the small number of measurements, high level of cloud cover, and large relative errors. The GEOS-Chem NH$_3$ VCD over South Korea was significantly lower than the IASI levels in June and July due to no monthly variation in REAS NH$_3$ emissions. The GEOS-Chem NH$_3$ VCD over the Kanto region indicated a more significant seasonal variation than that revealed by IASI retrievals, and was consistent with REAS emissions, indicating the importance of Japanese domestic emissions. Over the Kyushu region, the GEOS-Chem NH$_3$ VCD peaked in May, while REAS emissions did not, which may indicate the effect of the long-range transport of NH$_3$ from outside Japan. Based on a sensitivity simulation by GEOS-Chem, we found that only 35% of the NH$_3$ (in May) in the Kyushu region originated from domestic emissions.

4.2 Comparisons between JELA-FP Data and IASI and GEOS-Chem Results

Figure 5 shows the annual averaged FP-NH$_3$ data over Japan and a comparison with IASI NH$_3$ and GEOS-Chem NH$_3$ VCDs. Figure 6 shows a scatter plot of (a) FP-NH$_3$ and GEOS-Chem surface NH$_3$, (b) FP-NH$_3$ and GEOS-Chem NH$_3$ VCD, (c) FP-NH$_3$ and IASI NH$_3$, and (d) IASI and GEOS-Chem NH$_3$ VCDs for observations made in 2014. Figure 6 also shows a comparison of IASI and GEOS-Chem results over (e) north and central China, and (f) south China.
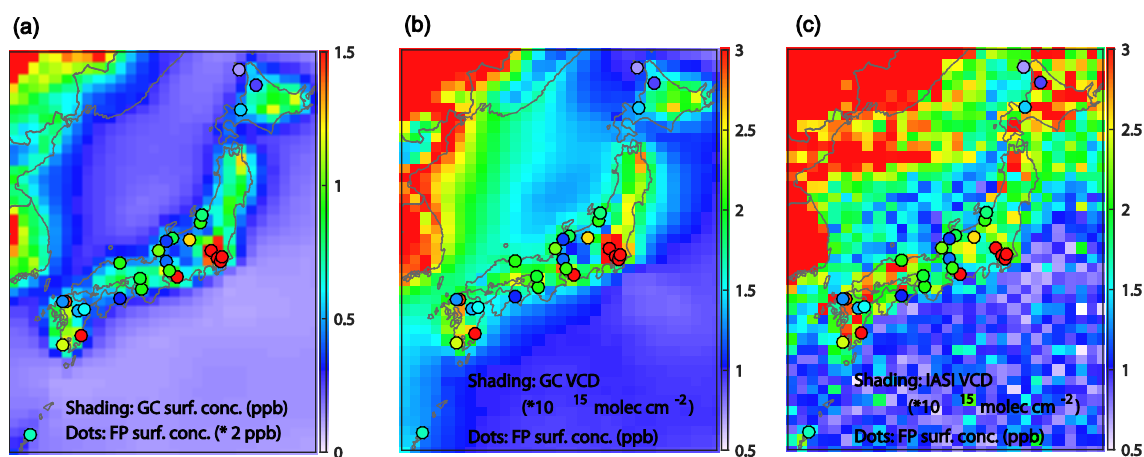

Fig. 5 Annual averaged FP-NH$_3$ data over Japan and a comparison with (a) GEOS-Chem surface concentration, (b) GEOS-Chem NH$_3$ VCD, and (c) IASI NH$_3$ VCD.
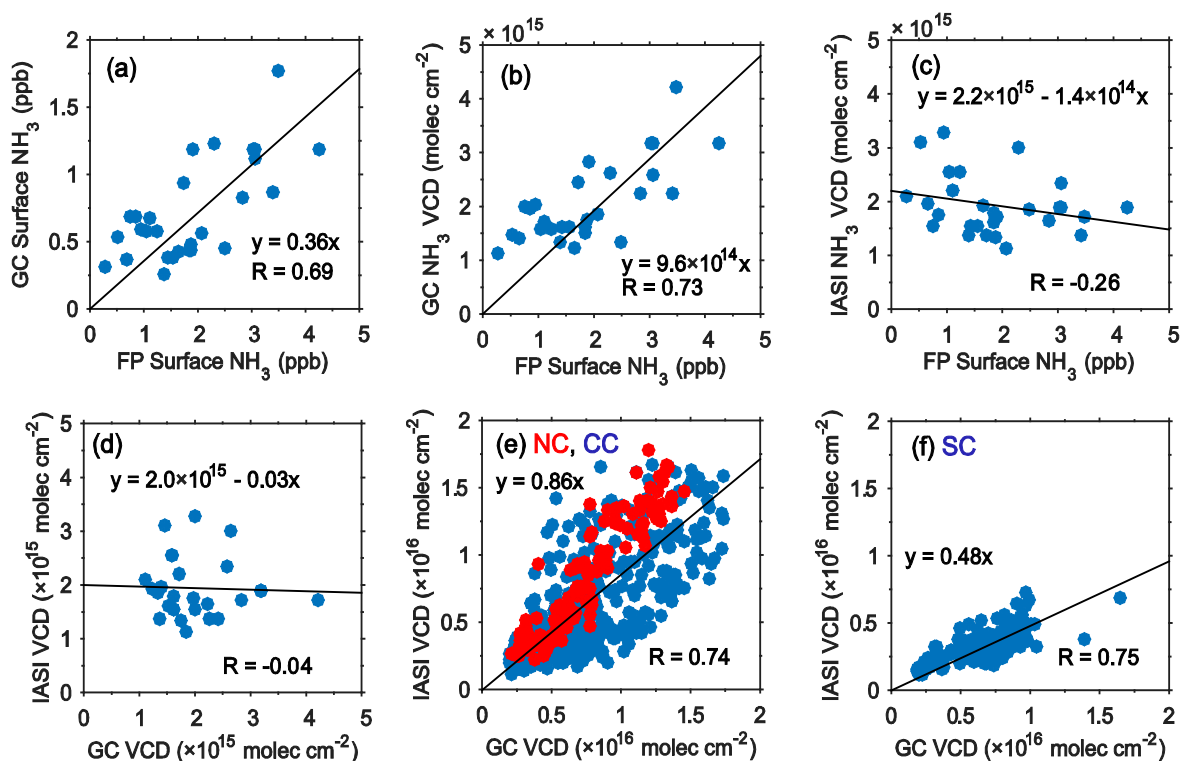
Fig. 6 Scatter plot of (a) FP-NH₃ and GEOS-Chem surface NH₃, (b) FP-NH₃ and GEOS-Chem NH₃ VCD, (c) FP-NH₃ and IASI NH₃, (d) IASI and GEOS-Chem NH₃ VCDs, (e) IASI and GEOS-Chem NH₃ VCDs for north (red dots) and central (blue dots) China, and (f) IASI and GEOS-Chem NH₃ VCDs for south China.

FP and GEOS-Chem results shows the high correlation (R = 0.69), even if GEOS-Chem NH₃ is underestimated. High values of FP-NH₃ (and REAS) over the Kanto region were due to anthropogenic emissions and agriculture sectors. There were high values of FP-NH₃ over southern Kyushu, which were due to the large numbers of livestock and high levels of fertilizer use in local agriculture. IASI data did not indicate high values over the Kanto region, but did show higher values over Hokkaido, which was a different pattern to that indicated by the FP and GEOS-Chem results in winter. Scatter plots of the IASI NH₃ did not show a positive relationship with FP-NH₃ (the slope was negative, R = −0.26) and GEOS-Chem NH₃ VCD (slope was −0.03, R = −0.04), due to high relative errors over Japan. Scatter plots for north and central China indicated a relatively strong correlation (R = 0.74), due to there being sufficient IASI observations over these regions. There was a similar correlation (R = 0.75) over south China, although IASI retrieval was only 48% of the CTM value.

For a detailed time series comparison, we used two sites (S1 and S2) over the northern Hokkaido Region (Fig. 7) and five sites (S8–10, S13) over the Kanto Region (Fig. 8). The FP data variation range of S1 and S2 for the period of 2010 to 2014 is shown in the shaded area (Fig. 7a). The range of the IASI NH₃ VCD variation at S1 and S2 in 2014 is
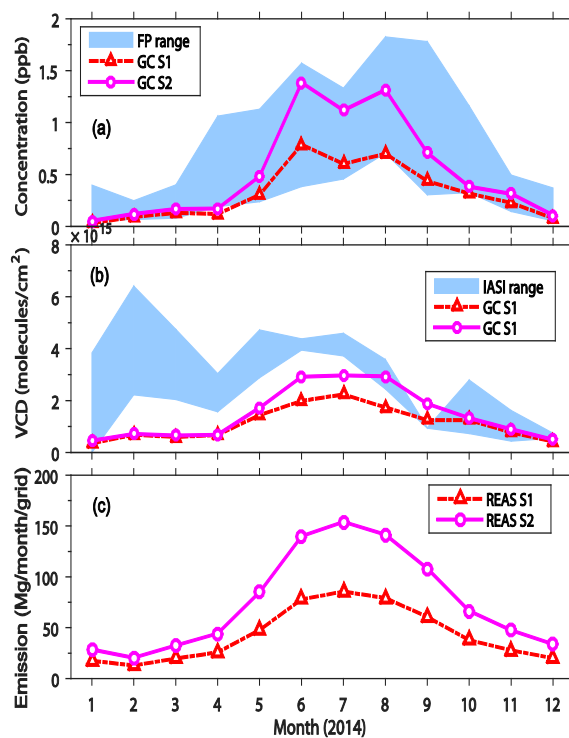

Fig. 7 Time series comparison for the Hokkaido region (S1 and S2), (a) FP-NH₃ concentration and GEOS-Chem surface concentration, (b) IASI NH₃ VCD and GEOS-Chem NH₃ VCD, (c) REAS NH₃ emissions for the S1 and S2 grid points. Grid = 0.5° × 0.667°.

indicated in Fig. 7b by the shaded area. The FP and GEOS-Chem results showed similar seasonal variation, and the GEOS-Chem NH_3 range had a reasonable agreement with FP data. The winter peak in IASI data (January to March) was unexpected due to the relatively large cloud cover and limited observation data (Fig. 3d).

Figure 8 shows similar information for the Kanto area. FP data for various sites (7, 8, 9, 10, and 13 for 2014) are shown in the shaded area. The FP average was higher than the GEOS-Chem average (GEOS-Chem was underestimated), but both displayed a clear summer peak (seasonal cycle). FP and GEOS-Chem had a peak in August, but there was no peak in IASI data at this time. There was a July peak in REAS emission data. The IASI results in August indicated very low levels, and did not show a significant summer maximum, which may be due to large relative error.

4.3 Impact of Local NH_3 Emissions at the Dazaifu and Fukuoka Sites

FP observations in Fukuoka Prefecture were conducted at two sites. S26 (Dazaifu) was located in FIHES (Fukuoka Institute of Health and Environmental Sciences) near the CC–KU, while S27 (Fukuoka, elevation = 170 m) was located in a rural area of Fukuoka city (about 13 km southwest of the Fukuoka downtown area and surrounded by small forest), and therefore was not influenced by urban activity. The locations of these two sites are shown in Figs. 1 and A.3), which clearly show the differences in NH_3 emissions. The emission rates at the Dazaifu, CC–KU, and Fukuoka sites were 3.68, 2.22, and 0.26 ton/km²/year, respectively.

Figure 9a shows FP data for Fukuoka and Dazaifu for 2014 and a box-whisker plot of NH_3 measurements at CC–KU (monthly data for January–July 2015, and August–December 2014 was used to show the seasonal cycle). Figure 9b and 9c show a comparison of IASI and GEOS-Chem NH_3 VCDs over Fukuoka and REAS NH_3 emissions used for GEOS-Chem simulations (the horizontal resolution of the REAS emission inventory was approximately 50 km; therefore, the Dazaifu and Fukuoka sites could not be distinguished), respectively. The FP NH_3 levels were highest at Dazaifu, which may be due to strong local NH_3 emissions.

The CC–KU NH_3 observations were compared with measurements made at Fukuoka (S27) and Dazaifu (S26). This indicates that differences in local NH_3 emissions around the observation site played an important role in the observed NH_3 concentrations, even when two measurement sites were located in the same GEOS-Chem grid. Both the NH_3 surface
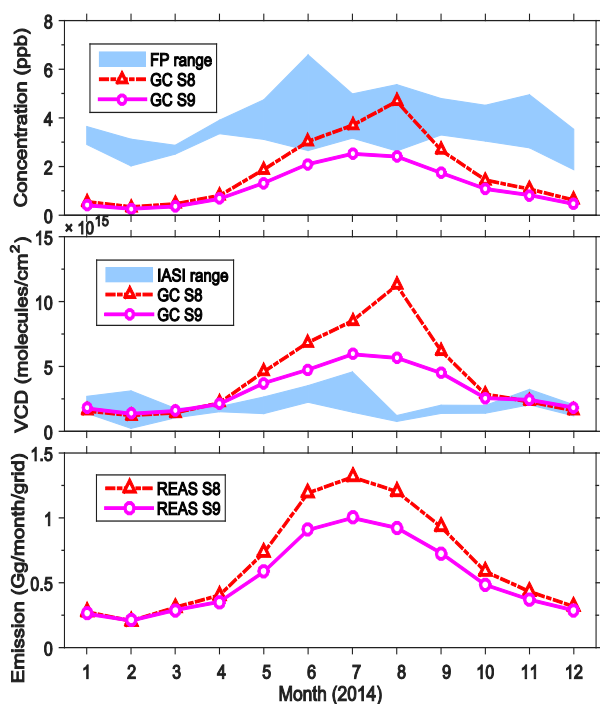
Fig. 8 Time series comparison for the Kanto region (a) FP-NH_3 concentration and GEOS-Chem surface concentration, (b) IASI NH_3 VCD and GEOS-Chem NH_3 VCD, and (c) REAS NH_3 emissions for S8 and S9 grid points. FP data for sites 8–10 and 13 for year 2014 are shown in the shaded area. Grid = 0.5° × 0.667°.
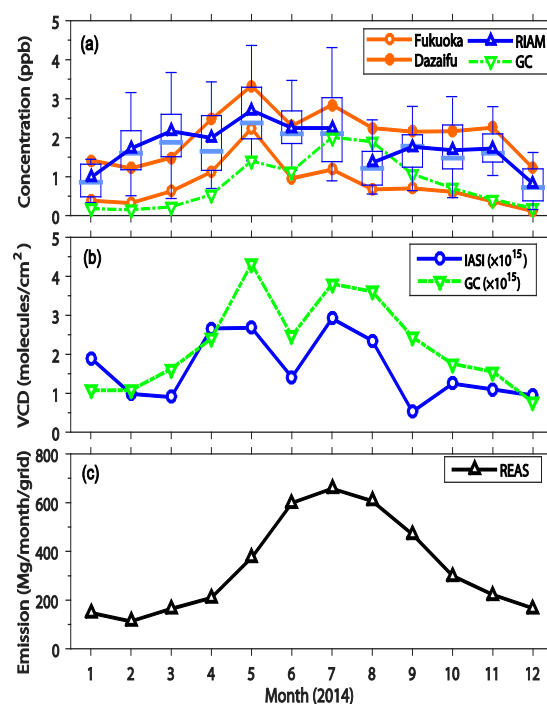
Fig. 9 (a) Time series of FP data for Fukuoka and Dazaifu for 2014 and a box-whisker plot of NH_3 measurements at CC–KU (monthly data for January – July 2015, and August – December 2014 was used), (b) comparison of IASI and GEOS-Chem NH_3 VCDs over Fukuoka, and (c) REAS NH_3 emissions used for GEOS-Chem simulation. Grid = 0.5° × 0.667°.

concentration and VCD produced by GEOS-Chem displayed peaks in May and July. The peaks in GEOS-Chem NH$_3$ surface concentration and VCD occurred in different months. The GEOS-Chem surface concentration peaked in summer, while the GEOS-Chem VCD peaked in May. This may be because the long-range transport of NH$_3$ occurs in elevated layers in spring. The IASI NH$_3$ VCD differed between Fukuoka and Kyushu, as shown in Fig. 4. The Kyushu NH$_3$ VCD had a peak in summer, but there was no peak in May (this may be due to the differences in the average area of IASI observation data).

5. Conclusions

Atmospheric ammonia (NH$_3$) plays an important role in the formation and understanding of secondary inorganic aerosols, but has not been examined using chemical transport models (CTMs), and atmospheric levels have not been compared with satellite observations in Japan. We analyzed the seasonal variation in atmospheric NH$_3$ using long-term hourly NH$_3$/NH$_4^+$ measurements made at CC-KU in Fukuoka, the nationwide FP network observation, GEOS-Chem CTM results, and IASI satellite retrievals over East Asia.

IASI NH$_3$ data provided useful information for East Asia. IASI retrievals over central and north China were similar to the CTM results. However, over south China, there were fewer IASI observations due to high levels of cloud cover and the retrieval results were underestimated compared with CTM results (IASI NH$_3$ was 48% of CTM NH$_3$).

Over Japan, the Japan nationwide FP-NH$_3$ data from JELA and CTM results were strongly correlated (R = 0.65) even when CTM results were underestimated (in about half of the FP measurements). It was found that the IASI observations over Japan were below or near the detection limit and it was difficult to obtain a reasonable correlation between surface measurements and CTM results.

Data from two FP-NH$_3$ measurement sites within Fukuoka Prefecture were examined carefully. Dazaifu FP-NH$_3$ measurements displayed a clear seasonal cycle (spring-summer high and winter low), and was 2–3 times higher than that of the Fukuoka rural site (located 13 km southwest of the Fukuoka downtown area). The NH$_3$ measurements at CC-KU were compared with FP-NH$_3$ measurements at the Dazaifu and Fukuoka sites. Estimated NH$_3$ emissions with 1-km resolution identified a 10-fold difference in levels between the Dazaifu and Fukuoka sites (Dazaifu was higher, Figs. 1 and A.3). This indicates that differences in local NH$_3$ emissions around an observation site play an important role in determining the observed NH$_3$ concentrations. The CTM underestimation (by about 50%)

can be understood by the underestimation of the NH$_3$ emission inventory (50-km resolution) used in the CTM simulation.
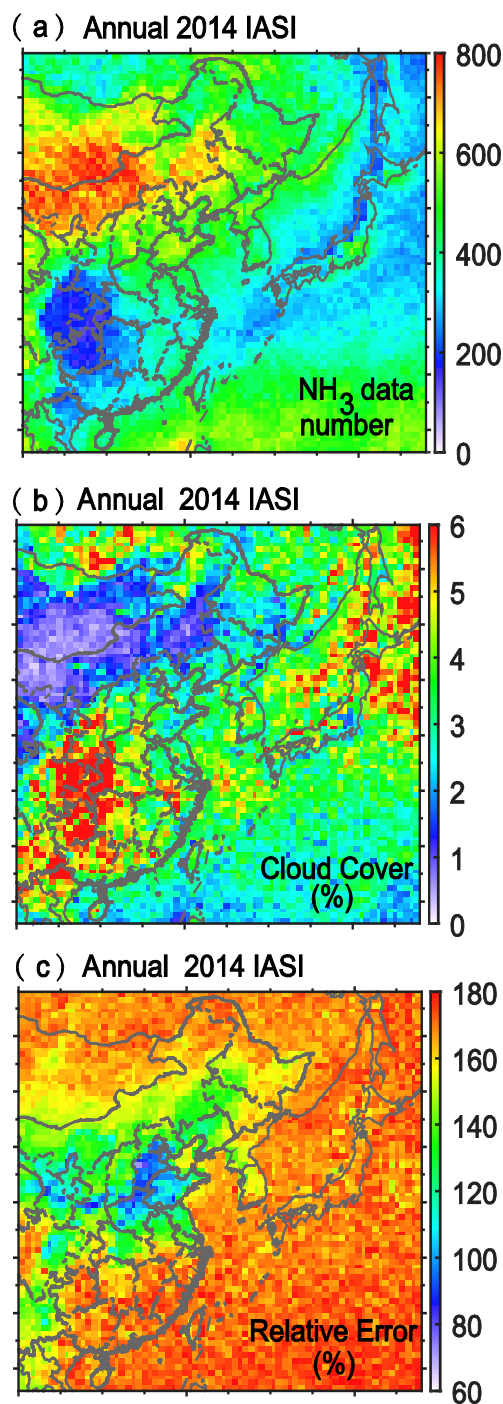
Appendix

Fig. A1 Annual averaged distribution of (a) data points, (b) cloud cover (%), and (c) relative error (%).
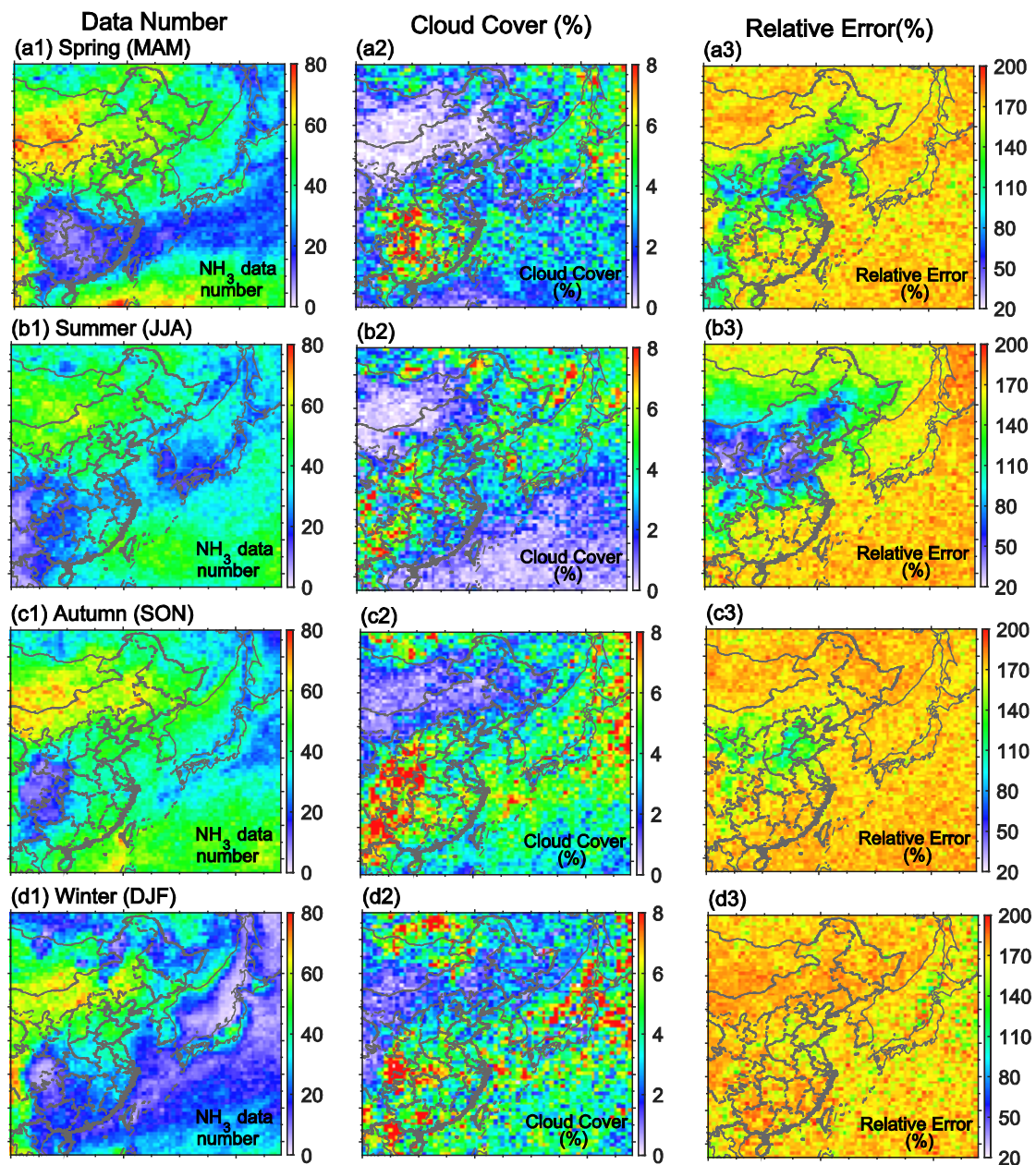
Fig. A2 Same as Fig. A.1, but for different seasons.

Appendix A.3 EAGrid NH$_3$ Distributions

In the EAGrid inventory [21], NH$_3$ emissions were estimated mainly by a top-down approach using the activity data from sources (livestock, fertilizer applications, leakage in the fertilizer production process, pet dogs, human perspiration, vehicles, and latrines), with a 1 km^2 horizontal resolution. Ammonia emissions originating from livestock were estimated from the numbers of six types of livestock contained in village statistics. Seasonal and diurnal variation patterns of volatilization were based on the previous literature [22].

Figure A.3 shows the annual averaged NH$_3$ emission from (a) all sources, (b) the agriculture sector, (c) humans and pets, and (d) the automobile sector. It can be clearly seen that the NH$_3$ emissions from agriculture (humans and pets) accounted for 48.0% (33.7%) of total NH$_3$ emissions. It also shows that the automobile contribution accounted for 14.7% of emissions near the Fukuoka downtown area.

The seasonal variation in NH$_3$ emissions from each sector is of interest. Figure A.4 shows the monthly variation in NH$_3$ emissions averaged over the area shown in Fig. A.3. It was found that the NH$_3$ emission from the agricultural sector shows significant seasonal variation, as does the human and pet sector, while there is no seasonal variation in the automobile sector.
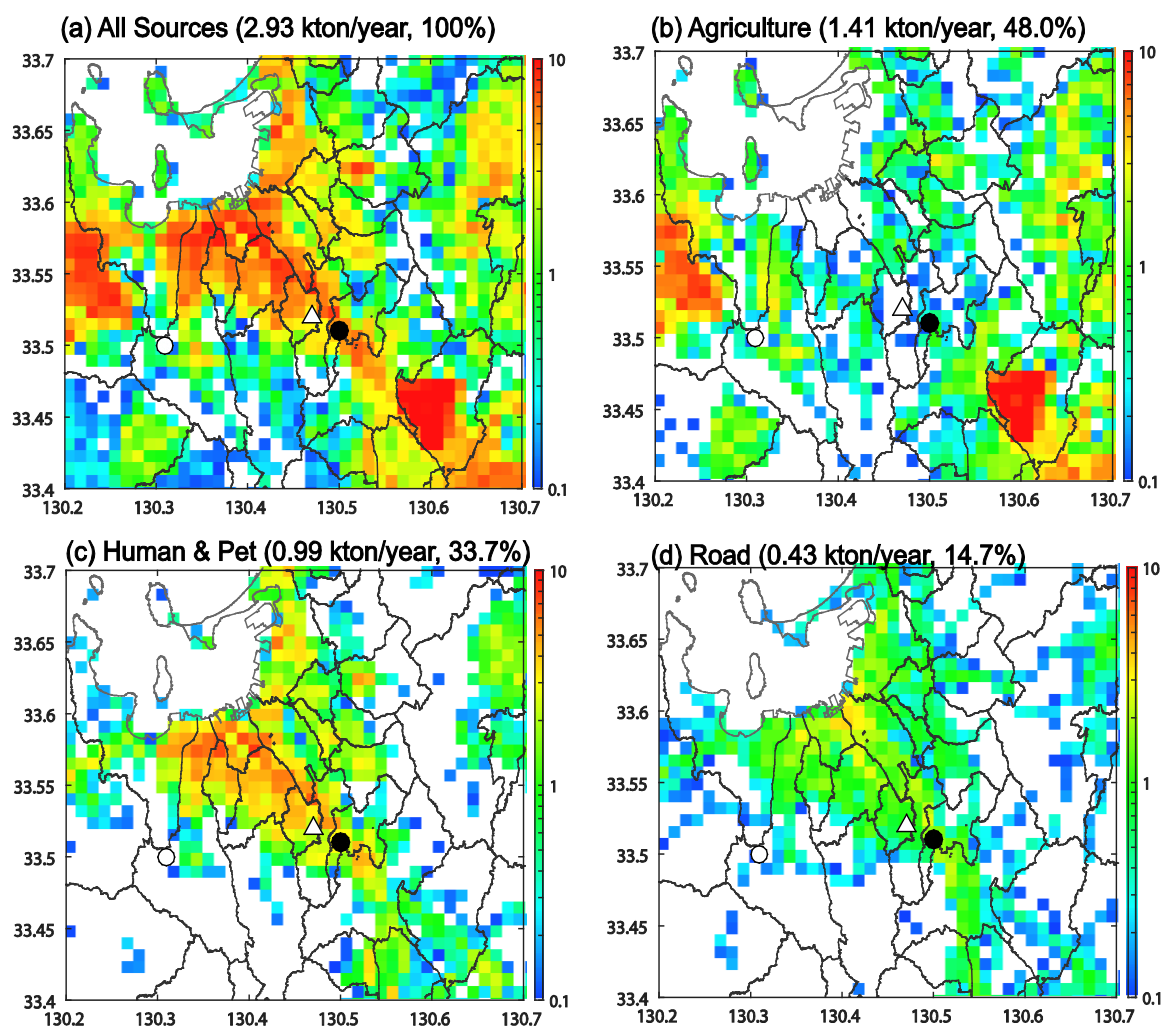
(a) All Sources (2.93 kton/year, 100%)

(b) Agriculture (1.41 kton/year, 48.0%)

(c) Human & Pet (0.99 kton/year, 33.7%)

(d) Road (0.43 kton/year, 14.7%)

Fig. A3 Annual averaged NH_3 emission from: (a) all sources, (b) the agricultural sector, (c) humans and pets, and (d) the automobile sector.

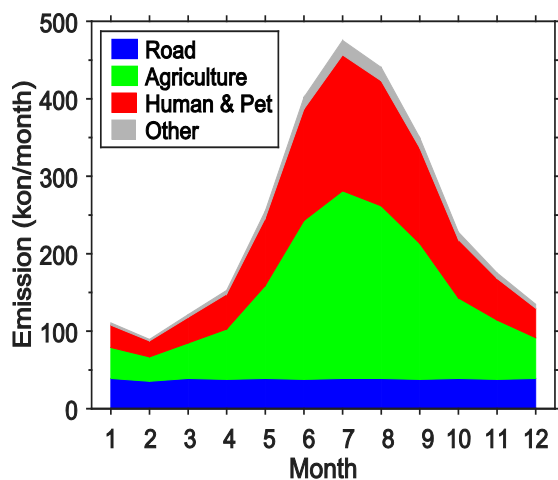Fig. A4. Monthly variation of NH_3 emissions averaged over the area shown in Fig. A3.

Acknowledgements

References

1)   Fowler, D., Coyle, M., Skiba, U., Sutton, M. A., Cape, J. N., Reis, S., Sheppard, L. J., Jenkins, A., Grizzetti, B., Galloway, J. N., Vitousek, P., Leach, A., Bouwman, A. F., Butterbach-Bahl, K., Dentener, F., Stevenson, D., Amann, M., and Voss, M.: The global nitrogen cycle in

the twenty-first century, Philos. Trans. R. Soc. London, Ser. B, 368, 1621, 2013.

2) Behera, S., Sharma, M., Aneja, V., and R., B.: Ammonia in the atmosphere: a review on emission sources, atmospheric chemistry and deposition on terrestrial bodies., Environ. Sci. Pollut. Res. Int., 20, 8092–131, 2013.

3) Erisman, J. W., Bleeker, A., Galloway, J., and Sutton, M.: Reduced nitrogen in ecology and the environment, Environ. Pollut., 150, 140–149, 2007.

4) Sutton, M. A., Erisman, J.W., Dentener, F., and Müller, D.: Ammonia in the environment: From ancient times to the present, Environ. Pollut., 156, 583–604, 2008.

5) Clarisse, L., Clerbaux, C., Dentener, F., Hurtmans, D., and Coheur, P.-F.: Global ammonia distribution derived from infrared satellite observations, Nat. Geosci., 2, 479–483, 2009.

6) Van Damme, M., Clarisse, L., Heald, C. L., Hurtmans, D., Ngadi, Y., Clerbaux, C., Dolman, A. J., Erisman, J. W., and Coheur, P. F.: Global distributions, time series and error characterization of atmospheric ammonia (NH_3) from IASI satellite observations, Atmos. Chem. Phys., 14, 2905–2922, 2014.

7) Osada, K., T. Kamikuchi, S. Yamamoto, S. Kuwahara, X. Pan, Y. Hara, I. Uno: Comparison of ionic concentrations on size-segregated atmospheric aerosol particle based on a denuer-filter method and a Continuous Dichotomous Aerosol Chemical Speciation Analyzer (ACA-12), Earozoru Kenkyu, 31, 203–209, 2016 (in Japanese with English abstract).

8) Itahashi, S., Uno, I., Osada, K., Kamiguchi, Y., Yamamoto, S., Tamura, K., Wang, Z., Kurosaki, Y., Kanaya, Y.: Nitrate transboundary heavy pollution over East Asia in winter, Atmos. Chem. Phys., 17, 3823-3843, 2017.

9) Wang Z., I. Uno, K. Osada, X. Pan, S. Yamamoto and Y. Kanaya. Observations of Aerosols and Trace Gases around the Chikushi Campus of Kyushu University. Reports of Research Institute for Applied Mechanics, 153, xx-xx, 2017.

10) Japan Environmental Laboratories Association (JELA), http://db.cger.nies.go.jp/dataset/acidrain/ja/05/data.html. [in Japanese]. 2016.

11) Van Damme, M., Clarisse, L., Heald, C. L., Hurtmans, D., Ngadi, Y., Clerbaux, C., Dolman, A. J., Erisman, J. W., and Coheur, P. F.: Global distributions, time series and error characterization of atmospheric ammonia (NH_3) from IASI satellite observations, Atmos. Chem. Phys., 14, 2905-2922, 2014.

12) Van Damme, M., Wichink Kruit, R. J., Schaap, M., Clarisse, L., Clerbaux, C., Coheur, P.-F., Dammers, E., Dolman, A. J., and Erisman, J. W.: Evaluating four years of atmospheric ammonia (NH_3) over Europe using IASI satellite observations and LOTOS-EUROS model results, J. Geophys. Res.-Atmos., 119, JD021911, 2014.

13) Bey, I., J. Jacob, R. M. Yantosca, A. Logan, B. D. Field, A. M. Fiore, Q. Li, H. Y. Liu, J. Mickley, and M. G. Schultz: Global modeling of tropospheric chemistry with assimilated meteorology: Model description and evaluation, J. Geophys. Res., 106, 73–95, 2001.

14) Park, R. J., Jacob, D. J., Field, B. D., Yantosca, R. M., Chin, M.: Natural and transboundary pollution influences on sulphate-nitrate-ammonium aerosols in the United States: implications for policy, J. Geophys. Res., 109, D15204, 2000.

15) Olivier, J.G.J. and J.J.M. Berdowski, Global emissions sources and sinks. In: Berdowski, J., Guicherit, R. and B.J. Heij (eds.) The Climate System, 33-78. A. A. Balkema Publishers/Swets & Zeitlinger Publishers, Lisse, The Netherlands, 2001.

16) Kurokawa, J., Ohara, T., Morikawa, T., Hanayama, S., Janssens-Maenhout., G, Fukui, T., Kawashima, K., Akimoto, H.: Emissions of air pollutants and greenhouse gases over Asian regions during 2000–2008: Regional Emission inventory in ASia (REAS) version 2, Atmos. Chem. Phys., 13, 11019–11058, 2013.

17) Huang, X., Song, Y., Li, M., Li, J., Cai, X., Zhu, T., Hu, M., Zhang, H.: A high-resolution ammonia emission inventory in China, Global Biogeochem. Cycles, 26, GB1030, 2012.

18) Xu, P. et al.: An inventory of the emission of ammonia from agriculture fertilizer application in China for 2010 and its high-resolution spatial distribution, Atmos. Environ. 115, 141–148, 2015.

19) Uno, I., Yumimoto, K., Pan, X. L., Wang, Z., Osada, K., Itahashi, S., Yamamoto, S.: Simultaneous dust–pollutants transport over East Asia: the Tripartite Environment Ministers Meeting March 2014 Case Study, SOLA, 13, 47-52, 2017.

20) Uno, I., K. Yumimoto, K. Osada, Z. Wang, X.L. Pan, S. Itahashi and S. Yamamoto: Dust Acid Uptake Analysis during Long-lasting Dust and Pollution Episodes over East Asia based on Synergetic Observation and Chemical Transport Model, SOLA, 13, 109-113, 2017.

21) Kannari, A., Tonooka, Y., Baba, T., Murano, K. Development of multiple-species 1km×1km resolution hourly basis emissions inventory for Japan, Atmos. Environ., 41, 3428-3439, 2007.

22) Asman, W. A. H. Ammonia emission in Europe: Updated emission and emission variation. Report No. 228471008, National Institute of Public Health and Environmental Protection, Bilthoven, 1992.